SEARCH RESULTS [PDF Full-Text (260 KB)] PREVIOUS NEXT

New Fast **GPS** code-acquisition technique using **FFT**

- *Van Nee, D.J.R.; Coenen, A.J.R.M.*
Delft Univ. of Technol., Netherlands

This paper appears in: **Electronics Letters**
On page(s): 158 - 160
17 Jan. 1991
Volume: 27 Issue: 2
ISSN: 0013-5194
References Cited: 4
CODEN: ELLEAK
INSPEC Accession Number: 3846752

Abstract:
A new spread-spectrum code-acquisition technique for the navigation systems Navstar/**GPS** and Glonass is introduced. This technique uses the **FFT** to compu correlation function, thereby eliminating the time-consuming code phase shift p Comparisons with existing systems show a theoretical reduction in acquisition t about 2000 times.

Index Terms:
fast Fourier transforms; Glonass navigation system; **FFT**; spread-spectrum code-acquisition technique; navigation systems Navstar/**GPS**; correlation funct acquisition time; correlators; encoding; fast Fourier transforms; radionavigatio spectrum communication

SEARCH RESULTS [PDF Full-Text (260 KB)] PREVIOUS NEXT

length ratios of u/L, v/L and w/L are 0·3, 0·4, and 0·3, respectively. As indicated in Fig. 2, more than -20dB crosstalk level of bar state can be expected over the range from 3 to 4 of $\Delta\beta_{TM}/\Delta\beta_{TE}$. By designing the length of each section (u, v, w) adequately, a voltage controlled optical power splitter can be produced as shown in Fig. 3. Uniform $\Delta\beta$ elements, whose L/l_{TM} and L/l_{TE} were about 1 and 3, were used to measure the ratio a. The measured ratio a was from 3·6 to 3·8 in our experiment and was bigger than the previously reported values.[3,5] This is presumably due to the difference in mode confinement conditions for TM and TE modes between measured directional couplers. However, a of around 3·7 is favourable for the performance of the device proposed.

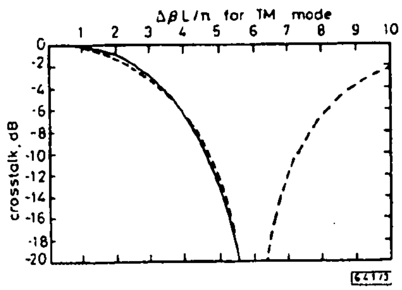

Fig. 3 *Calculated characteristics as optical power splitter*
$u/L = 0.3675$; $v/L = 0.265$; $w/L = 0.3675$; $a = 3.6$

Fabrication: The coupling length conditions for the TM and TE modes were satisfied when 750 Å-thick titanium, 7 μm width, and 7 μm spacing patterns were diffused at 1050°C for 6 h in a wet Ar atmosphere. The length of each section was determined based on the measured $\Delta\beta_{TM}/\Delta\beta_{TE}$. The coupling effects of the curved guide regions ($R = 40$ mm) at the both sides of directional couplers for the TM and TE modes were also considered to define electrode photomask patterns. These coupling effects were measured by comparing the output light intensities from the guides of directional couplers with theoretical values, and their estimated values in terms of coupling length were less than 1 mm for both modes. From these fundamental data, devices with the length ratios of $u/L = 0.375$, $v/L = 0.25$, and $w/L = 0.375$ ($L = 22$ mm) were fabricated for optical power splitters.

Experimental results: The device characteristics were measured by PMF endfire coupling at 1·31 μm wavelength. A computer controlled measurement system with a IR camera and a voltage generator was used. Digital video signals from

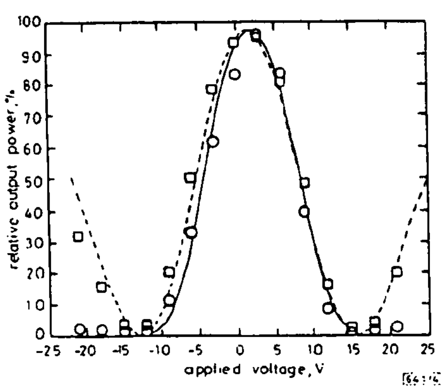

Fig. 4 *Measured and calculated characteristics*
○ measured for TM mode
□ measured for TE mode
—— TM mode
- - - - TE mode
$u/L = 0.375$; $v/L = 0.25$; $w/L = 0.375$; $a = 3.5$; $L = 22$ mm

the IR camera were integrated and computed to measure crosstalk values.

Fig. 4 shows the measured optical output intensities for both polarisations as functions of the applied voltages. In the Figure, calculations are also plotted. The ratios of the coupling length to the complete coupling lengths were about 0·9 for the TM mode and about 2·9 for the TE mode. As predicted by the calculations, the switching voltages for the TM and TE modes are coincident, and the applied voltage dependence of the output light intensities for the TM mode is also coincident with that for the TE mode. The switching voltage is relatively low, about 15 V.

Conclusion: New polarisation-insensitive devices, based on the modified configuration of three section alternating $\Delta\beta$, have been produced in Z-cut $LiNbO_3$. Polarisation-insensitive switching and power splitting characteristics have been obtained.

N. KUZUTA
K. TAKAKURA
Shimadzu Co. Opto-electronics Department
2385-13 Ihiyama Atsugi, Kanagawa 243-02, Japan

26th November 1990

References

1 OKAYAMA, H., MATUBA, A., SHIBUYA, R., and ISHIDA, T.: 'Polarisation independent optical switch with cascaded optical switch matrices', *Electron. Lett.*, 1988, **24**, pp. 959–960
2 GRANESTRAND, P., LAGERSTRÖM, B., SVENSSON, P., THYLEN, L., STOLTZ, B., BERGVALL, K., and OLOFSSON, H.: 'Tree-structured polarisation independent 4 × 4 switch matrix in $LiNbO_3$', *Electron. Lett.*, 1988, **24**, pp. 1198–1200
3 KONDO, M., OHTA, Y., TANISAWA, T., AOYAMA, T., and ISHIKAWA, R.: 'Low-drive-voltage and low-loss polarisation independent $LiNbO_3$ optical waveguide switches', *Electron. Lett.*, 1987, **23**, pp. 1167–1169
4 KOGELNIK, H., and SCHMIDT, R. V.: 'Switched directional coupler with alternating $\Delta\beta$', *IEEE J. Quantum Electron.*, 1976, **QE-12**, pp. 396–401
5 HABARA, K.: '$LiNbO_3$ directional coupler polarisation splitter', *Electron. Lett.*, 1987, **23**, pp. 614–616

NEW FAST GPS CODE-ACQUISITION TECHNIQUE USING FFT

Indexing terms: Correlation, Fast Fourier transforms

A new spread-spectrum code-acquisition technique for the navigation systems Navstar/GPS and Glonass is introduced. This technique uses the FFT to compute the correlation function, thereby eliminating the time-consuming code phase shift process. Comparisons with existing systems show a theoretical reduction in acquisition time of about 2000 times.

Introduction: A short acquisition time is very important for a standard positioning service Navstar/GPS or Glonass receiver, especially in an urban environment where satellites are often visible for a few seconds only. In this case, an acquisition time of less than a few seconds is desired to avoid the receiver having to continuously remain in the acquisition phase. We discuss the code acquisition time only, that is, the time needed to align the incoming code and the local code within one chip. The proposed new acquisition technique is a result of our research into satellite navigation in an urban environment.

Noncoherent correlator: The most frequently used code acquisition system is the noncoherent correlator, shown in Fig. 1.[1,2] The incoming signal $x(t)$ consists of noise plus the GPS signals which have a carrier frequency of 1·6 GHz, and are binary phase modulated by a Gold sequence of 1023 chips with a chip rate of 1 MHz, and by a 50 Hz data stream. This signal is converted to baseband and coherently correlated with the local code for NLT_c seconds. Here L is the code length

(= 1023 chips for the C/A code), T_c is the chip time and N is an integer ≥ 1. This time is chosen short enough to ensure that the presence of data and carrier Doppler shift will not cause a great degradation in performance.[3] Next, K sequential correlations are noncoherently summed to produce one correlation point at a sufficiently high signal-to-noise ratio. The total integration time $KNLT_c$ is called the dwell time.

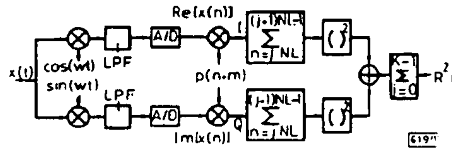

Fig. 1 *Noncoherent correlator in time domain*

To achieve acquisition with the noncoherent correlator, the above procedure has to be performed for all possible code phases and also for a number of possible Doppler frequencies, because the carrier phase has to remain nearly constant during individual integration times NLT_c. As a result, the acquisition time is proportional to the number of cells, which is defined as the product of the number of code phase steps and the number of carrier frequency steps. For GPS, a typical value of the number of cells is 20460 for half a chip phase step (2046 steps for the C/A code) and 1 kHz carrier frequency step at a correlation time of 1 ms ($N = 1$) and a carrier Doppler range of 10 kHz, neglecting the contribution due to the speed of the receiver.

Parallel search techniques using the FFT: To reduce the acquisition time, cells can be searched in parallel by taking the FFT of the complex samples at the points I and Q in Fig. 1.[3] At the moment that the incoming code and the local code have the same phase, a carrier component will be present in the spectrum, which is visualised by the FFT. Using this technique only 2046 phase steps remain, reducing the acquisition time ten times in comparison with the first system, assuming the FFT can be computed within the dwell time.

In the above system, a parallel search in frequency is performed to eliminate 10 frequency search steps. In our proposed system, a parallel search in time is performed, i.e. all points of the correlation function are calculated from the same input sequence, with a theoretical gain in acquisition time of 2046 times in comparison with the conventional correlator, which is much more than the gain of the previous system that also uses a digital signal processor, but in a completely different way.

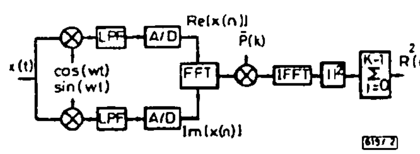

Fig. 2 *Noncoherent correlator via frequency domain*

The correlation operations are implemented as follows (see Fig. 2). A digital signal processor loads $2NL$ complex samples with a time spacing of half a chip and then performs the correlation operation

$$R(m) = \sum_{n=0}^{NL-1} x(n) \cdot p(n+m) \qquad \text{for } m = 0, 1, \ldots, 2L-1 \quad (1)$$

The processor stores all $2NL$ points of $R^2(m)$ in an accumulator. This process is repeated until K separate correlation functions have been summed.

Unfortunately, a straightforward calculation of $R(m)$ requires a large number of operations, which is proportional to $(NL)^2$. Much computing time can be saved, however, if the correlation function is calculated via the frequency domain:[4]

$$R(m) = x(n) * p(-n) = F^{-1}[X(k) \cdot \bar{P}(k)] \qquad (2)$$

where $*$ represents convolution, $X(k)$ is the spectrum of $x(n)$, $\bar{P}(k)$ is the complex conjugate of the spectrum of $p(n+m)$ and F^{-1} is the inverse Fourier transform.

The fastest FFT algorithms require the number of points to be radix 2. We therefore add two zeros in both incoming and local code with a spacing of half the code length. In fact, we slightly deform the codes, which yields the advantage of fast processing but has the disadvantage of a somewhat larger crosscorrelation. The latter effect, however, is negligible compared to the thermal noise level in the acquisition phase.

Because the digital signal processor computes the entire correlation function in one dwell time, this technique is theoretically 2046 ($2L$) times faster than the previously mentioned parallel frequency search method, which uses the same amount of hardware. In practice, this gain will only be achieved if the signal processor is fast enough to compute $2K$ times a $2NL$ point FFT within one dwell time. Also, this has to be done for at least ten different carrier frequency steps; for each frequency step the input signal is frequency shifted through a software-implemented image-rejection mixer. For the typical values $K = 20$, $N = 1$ and ten frequency steps, this would mean that ten 2048 point FFTs have to be computed within 500 µs. Such signal processors actually exist but are still extremely expensive. However, even with the TMS320C30 processor we use, an estimated minimum acquisition time of less than 500 ms per frequency step is possible, which then yields a gain in acquisition time of eight times compared to the parallel frequency search system. In the case of reacquisition, which will occur frequently in an urban environment, the carrier frequency will often be known accurately enough to reduce the number of frequency search steps to only one, so the gain in acquisition time of the TMS320C30 can be increased by a factor ten.

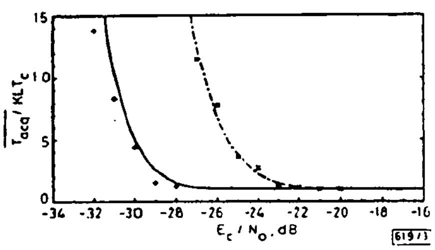

Fig. 3 *Normalised mean acquisition time as function of the signal-to-noise ratio for $K = 20$ and $K = 4$*

—— $K = 20$
— · — $K = 4$
+ simulated results for $K = 20$
× simulated results for $K = 4$
$L = 1023 \quad c = 5$

Finally, to demonstrate that the system actually works, Fig. 3 shows a plot of the mean acquisition time as a function of the signal-to-noise ratio E_c/N_0 which is calculated using the equations described in Reference 3. For a number of different signal-to-noise ratios, we simulated a GPS spread-spectrum signal with additive Gaussian noise. We performed 100 simulations for each value of the signal-to-noise ratio, and counted the number of successful acquisitions, which is a measure of the acquisition probability p that can be substituted in the equation for the mean acquisition time in the case of a single dwell acquisition procedure (for $N = 1$)

$$\frac{\overline{T_{acq}}}{KLT_c} = \sum_{i=0}^{\infty} [ic + (i+1)] \cdot (1-p)^i \cdot p = \frac{1 + c \cdot (1-p)}{p} \qquad (3)$$

The constant $c \cdot KLT_c$ is the penalty time in the case of a false alarm. As can be seen, the simulated plots have a close resemblance to the calculated curves. The shift of about half a dB for $K = 20$ is most probably due to the approximations in the calculation, so we can conclude that the performance of the systems in Fig. 1 and 2 are the same, except for a constant factor in the acquisition time. It should be noticed that the mean acquisition time in Fig. 3 is multiplied by a certain

factor if the signal processor used is not processing in real time.

Conclusions: By using a digital signal processor in a hitherto unusual way, the code acquisition time of a GPS receiver can be reduced considerably. The fastest performance is achieved when the incoming code and the local code are slightly deformed by adding zeros, allowing the use of the FFT.

Acknowledgment: The authors would like to thank Mr. E. Theunissen and Mr. T. Lamerigts for their work on the TMS320C30 processor and Prof. D. van Willigen and Prof. R. Prasad for their helpful comments.

D. J. R. VAN NEE
A. J. R. M. COENEN

Telecommunications and Traffic-control Systems Group
Delft University of Technology
PO Box 5031, 2600 GA Delft, The Netherlands

23rd November 1990

References

1 HOLMES, J. K.: 'Coherent spread spectrum systems' (Wiley, New York, 1982), p. 423
2 CHERUBINI, G., and PUPOLIN, S.: 'Performance analysis of an all digital acquisition circuit', *IEEE Trans. Commun.*, 1985, **33**, pp. 863–868
3 CHENG, U., HURD, W. J., and STATMAN, J. I.: 'Spread spectrum code acquisition in the presence of Doppler shift and data modulation', *IEEE Trans. Commun.*, 1990, **38**, pp. 241–250
4 OPPENHEIM, A. V., and SCHAFER, R. W.: 'Digital signal processing' (Prentice-Hall, New Jersey, 1975), p. 556

INJECTION-LOCKING OF Q-SWITCHED AlGaAs LASER WITH FAST SATURABLE ABSORBER

Indexing terms: Semiconductor lasers, Lasers

Injection of a weak CW laser beam in a Q-switched AlGaAs laser diode with a fast saturable absorber is shown to produce powerful single-mode picosecond pulses at 0·82 μm. The saturable absorber regions are obtained by deep implantation of heavy ions through the diode facets. Single-mode operation is achieved with CW injection powers as low as 50 μW. Peak powers exceeding 1·5 W are detected at the laser output. A time-resolved spectroscopy of the laser pulses reveals an overall downchirp of 1·5 nm.

Introduction: Q-switching of (Al)GaAs laser diodes is now recognised as being a very efficient and simple technique to produce picosecond pulses in the 0·8–0·85 μm region.[1–4] Recently, 5 ps pulses with peak powers up to 5 W have been observed by using fast saturable absorbers.[4,5] Pulses produced by this technique, however, generally exhibit poor spectral characteristics that are not desirable for a number of applications. We demonstrate the possibility of controlling the laser spectrum with the injection of a weak CW beam into the cavity. Owing to the use of a very fast saturable absorber, output powers are ten times higher than those reported in the previous works on injection-locking of pulsed semiconductor lasers.[6] Moreover, time-resolved spectroscopy of the single-mode laser pulses reveals a downchirp of very large amplitude, which enables us to predict the feasibility of bandwidth-limited subpicosecond pulses.

Experimental setup: The experimental setup is shown in Fig. 1. The semiconductor laser is a GaAs/AlGaAs gain-guided double-heterostructure already described in previous works.[3,5] The active region is 200 μm long. The emission wavelength is in the 820–830 nm range. Internal Q-switching is obtained by producing regions of a saturable absorber near the mirrors of the laser resonator by 18 MeV implantation of nitrogen ions. With electrical pump pulses of 40 V amplitude, 1·5 ns risetime and 100 kHz repetition rate, the laser emits multimode optical pulses of 5–10 ps full width at half maximum (FWHM). The energy per facet is 15 pJ.

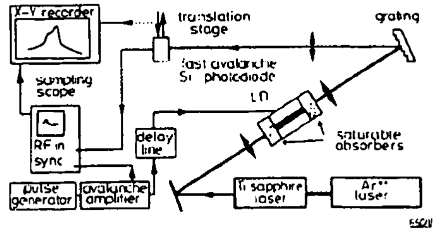

Fig. 1 *Experimental setup*

The laser mode control is presently achieved by injecting a weak CW tunable Ti : sapphire laser beam through one facet of the laser diode. A 0·1-NA $f = 20$ mm lens is used to focus the injection beam in the resonator. The CW infrared power incident onto the sample typically ranges from 10 to 100 μW, only 10% of which is estimated to be injected into the transverse resonator mode. The residual amount of power transmitted from the opposite facet of the laser diode is still one order of magnitude lower and typically represents less than 10% of the *average* output power delivered by the diode.

For spectral measurements, the output beam is diffracted with a 1200 g/mm grating after being collimated with a 0·35-NA $f = 10$ mm microscope objective. An $f = 50$ cm lens is then used to focus the diffracted beam either onto an infrared camera or a fast Si avalanche photodiode. The camera is used for rapid control of the laser spectrum. Injection-locking is seen to occur when one of the laser spots becomes much brighter than the others. For a more precise analysis, the camera is replaced by the fast photodiode, the latter having a detecting aperture of 50 μm. A spectral resolution of about 1 Å is obtained when scanning the photodetector across the beam.

The same arrangement is used to qualitatively analyse the wavelength evolution during the pulse. As shown in Fig. 1, the photodetector signal is fed into the 7S12 sampling unit of a Tektronix 7854 oscilloscope equipped with the S4 sampling head. Using the manual mode of operation, the signal is analysed in a temporal window of ~20 ps, the position of which can be adjusted with a precision of a few picoseconds with respect to the triggering pulse. The 7S12 unit output is then recorded while slowly scanning the photodetector across the diffracted beam. The operation is repeated for different positions of the temporal window. Because of the longer 100 ps response time of the photodetector as compared to the ~10 ps width (FWHM) of the optical pulses, the photodetector actually acts as an integrator. In other words, the procedure described above allows us to measure the time-averaged spectrum of the laser pulse for various averaging times in the tens of picoseconds scale. Although the resolution is limited by the width of the temporal window, we are able to determine the sign and the total amplitude of the wavelength shift during the pulse.

Experimental results: The efficiency of the injection-locking process is illustrated in Fig. 2. The bottom curve represents the multimode spectrum of the laser without injection. The pulse energy spreads over a dozen of the longitudinal modes, which approximately corresponds to a spectral width of 5 nm. The asymmetrical shape of the spectrum envelope indicates the presence of chirping effects. The top curve in Fig. 2 represents the laser spectrum under injection-locking conditions. Most of the pulse energy is now concentrated within a narrow spectral region located on the long wavelength side of the injection. The width of the spectral region essentially depends on the electrical pumping and typically ranges from 1·2 to 1·6 nm. The fraction of pulse energy contained within this region depends on the injection parameters. It increases with the injection power. At a given injection power, an optimum value is found when the injection is tuned near the gain maximum of the laser diode. For the case of Fig. 2, the injection power is 50 μW, the injection laser is tuned at 822 nm and